Global shape of the magnetotail current sheet as derived from Geotail and Polar data

N. A. Tsyganenko
Universities Space Research Association and Laboratory for Extraterrestrial Physics, NASA Goddard Space Flight Center, Greenbelt, Maryland

D. H. Fairfield
Laboratory for Extraterrestrial Physics, NASA Goddard Space Flight Center, Greenbelt, Maryland

Short title: WARPING/TWISTING OF THE TAIL CURRENT

Abstract. An analytical approximation is developed for the shape of the nightside tail current sheet, representing it as a function of the Earth's dipole tilt angle, solar wind ram pressure, and the interplanetary magnetic field (IMF). The model is based on 5-min average magnetometer data of the Geotail and Polar spacecraft, spanning the periods 1994–2002, and 1999–2001, respectively. All the magnetospheric data were tagged by concurrent values of the solar wind dynamic pressure and IMF B_y and B_z components, averaged over 30-min intervals immediately preceding the magnetospheric observations. Warping and twisting parameters were calculated by minimizing the number of mismatches between the observed and predicted orientation of the magnetic field on both sides of the model current sheet. The model is valid within the nightside magnetosphere in the range of tailward distances $-50\,R_{\rm E} \le X_{\rm GSM} \le 0$. Variations of the solar wind pressure P change the shape of the deformed current sheet in such a way that an increase of P results in a decrease of the magnetotail "hinging distance" $R_{\rm H}$, but increases the magnitude of its transverse warping. The IMF B_z component affects the magnitude of the seasonal/diurnal motion of the current sheet in the north-south direction, and it also controls the degree of the IMF B_y-related twisting, which becomes much larger during the periods with northward IMF B_z.

1. Introduction

The tail current sheet is a major source of the external magnetospheric field, and one of principal boundaries in the magnetosphere, defining its global geometry. Predicting the position of the tail current is important for the planning the science of magnetospheric missions and accurately interpreting their results. It is also crucial for the development of empirical models of the magnetospheric fields and plasmas.

The shape of the tail current sheet as a function of the dipole tilt and interplanetary conditions was addressed in numerous studies, using both magnetometer data [e.g., *Russell and Brody,* 1967; *Fairfield,* 1980; *Gosling et al.,* 1986; *Dandouras,* 1988; *Lopez* 1990; *Nakai et al.,* 1997; *Tsyganenko et al.,* 1998] and the plasma sheet particle data [*Owen et al.,* 1995]. These studies, based on different datasets and techniques, established main features of the current sheet geometry and quantified its location using various analytical approximations. The fundamental effect of the seasonal and diurnal oscillation of the dipole tilt angle is a periodic warping of the neutral sheet surface, so that it bends northward (or southward) near the midnight meridian, but moves in the opposite direction or stays at rest near the tail's flanks. The IMF B_y component was predicted [*Russell,* 1972] and found [*Sibeck et al.,* 1985] to exert a torque on the Earth's magnetotail, resulting in a left- or right-handed twisting of the cross-tail current sheet for positive or negative B_y, respectively.

A common shortcoming of all previous efforts is that they are limited to relatively narrow intervals of distance and they do not provide a global quantitative approximation of the deformed current sheet. Another limitation is the largely incomplete information on the effects of the variable interplanetary conditions, partially due to a limited coverage of the early magnetospheric observations by concurrent solar wind and IMF data. An effort to fill that gap was made by *Owen et al.* [1995], who analyzed the effects of the IMF B_y and B_z on the orientation of the plasma sheet using energetic ion data of ISEE-3, and by *Maezawa et al.* [1997], who used deep-tail plasma and magnetic field data of Geotail. However, their results were limited to the middle and distant tail, and no attempt was made to empirically represent the shape of the neutral sheet.

In our recent work [*Tsyganenko et al.,* 1998], the warping and twisting effects were quantitatively studied using a set of Geotail magnetometer data taken inside the magnetotail in the interval $-100 < X < -10\,R_{\rm E}$. The data were binned into 7 intervals of X, and the shape of the warped/twisted current sheet was found separately for

each bin by fitting a simple ”local” tail field model to the data. It was shown that the amplitude of the tilt-related motion of the midnight part of the current sheet did not decrease with tailward distance and remained at a nearly constant level up to $X \sim -100\,R_{\rm E}$. In contrast, the transverse warping was found to gradually fade away with the distance.

However, in that work we did not try to develop a unified empirical model that would analytically describe the deformation as a function of X. Neither was any attempt made to include effects of the solar wind ram pressure or those of the IMF B_z. In addition, we used a fitting criterion based on an oversimplified (Harris-type) tail field variation across the current sheet. As was shown in a later study [*Tsyganenko*, 1998], the warping in the YZ plane is accompanied by a north-south asymmetry of the lobe field magnitude, especially pronounced in the near-Earth tail. That effect could result in biased values of the warping parameters. Finally, much new data has become available, firstly, owing to the extended near-tail phase of the Geotail mission and, secondly, due to the gradual shift of the apogee of Polar to low latitudes, which made it possible to densely sample the inner magnetosphere inside $R = 9\,R_{\rm E}$, relatively poorly explored by previous missions.

The present work is intended to fill in the gaps left in earlier studies. Based on a new set of Geotail and Polar data, we derive here a model representing the shape of the tail neutral sheet on the nightside as a function of position along and across the tail, dipole tilt angle, solar wind ram pressure, and IMF B_y and B_z.

2. Data

Compared with previous studies of this kind, this work uses the largest set of observations, made in the low-latitude magnetosphere and covering the range of distances from 3 to 50 $R_{\rm E}$. It comprises magnetometer and plasma instrument data of Geotail taken between January 1994 and July 2002, and magnetometer data of Polar for the period from January 1999 to March 2002. All magnetospheric data records (5-min averages) have been tagged with concurrent values of the solar wind and IMF parameters, as detailed below.

2.1. Interplanetary Medium Data

As in our previous study based on Geotail observations [*Tsyganenko et al.,* 1998], the concurrent solar wind and IMF data are crucial not only for parameterizing the model, but also in the initial selection of the magnetospheric data. The interplanetary data came from ACE (1998–2002), WIND (1994–2002), and IMP 8 (1994–2000) observations. The original high-resolution data were initially averaged over 5-min intervals and extrapolated in space and time from spacecraft locations to Earth by using observed components of the solar wind velocity. From 1998 on, when both ACE and Wind data became available, we usually preferred Wind data, especially when the spacecraft was located closer to Earth than ACE. However, the percentage of Wind data used dropped significantly for the last few years because the orbital maneuvers made after 1999 often placed the spacecraft apogee far away from the Sun-Earth line. In this regard, we note that all data taken on solar wind streamlines passing farther than $\rho = 40\,R_{\rm E}$ from the Earth center were discarded, based on the observed deterioration of correlations in the solar wind data with growing ρ [e.g., *Richardson and Paularena,* 2001, and references therein]. More details on the solar wind data preparation can be found in our earlier publications [*Tsyganenko et al.,* 1999; *Tsyganenko,* 2002b].

Because of the well-known windsock effect, data-based studies of the magnetotail structure require an accurate information on the direction of the solar wind flow. As detailed below, before deriving the shape of the neutral sheet from the data, we converted the observed magnetospheric magnetic field vectors into the GSW coordinate system, whose X-axis is antiparallel to the actual direction of the solar wind at the observation time. In this regard, it is interesting to assess the extent of the typical deviation of the incoming solar wind from an average direction, aberrated by 4° from the Sun-Earth line. Figure 1 shows a histogram of the deviation angle Θ, calculated from three Cartesian components of the solar wind velocity, measured by IMP-8, WIND, and ACE during the period from 1994 to 2002. The histogram is based on 643,568 5-min average data records, and demonstrates that the 5%- median- and 95%- values of the deviation angle equal $\approx 0.8^\circ$, $\approx 3.1^\circ$, and $\approx 7.3^\circ$, respectively.

2.2. Magnetospheric Magnetic Field Data

As already noted, the magnetospheric observations covered both the inner low-latitude region (Polar data, $3 \leq R \leq 9\,R_{\rm E}$) and the more distant tail (Geotail data, $9 \leq R \leq 50\,R_{\rm E}$). In both cases, we started with 1-min resolution data. However, the processing procedures for the Geotail and Polar data were somewhat different, and hence we describe them below in two separate sections. Initially we also planned to add GOES-8, -9, and -10 magnetometer data to our dataset. However, it was soon realized that because of nearly fixed longitude position of the spacecraft relatively high above the geomagnetic equatorial plane, they almost never crossed the neutral sheet (more quantitatively, in less than $\sim 0.5\%$ of the total ≈40,000 hours of data) and hence could not provide any significant and reliable information on its position. Note that only nightside data were chosen for this study.

2.2.1. Geotail Data. Magnetic field data of Geotail served as a principal source of information on the shape of the neutral sheet. The original data were first merged into yearly files and corrected for a small B_z offset (see [*Tsyganenko*, 2002b] for more details). The next step was to filter out solar wind/magnetosheath intervals, using the magnetopause model by *Shue et al.* [1998], driven by concurrent solar wind data (hence, this procedure automatically discarded Geotail data without the solar wind/IMF information). After that the 1-min data were averaged over 5-min intervals and converted into the GSM coordinate system.

To further ensure that the Geotail magnetic field data were not contaminated by magnetosheath intervals we took the advantage of the availability of simultaneous LEP plasma instrument data and rejected all intervals with at least one of the following conditions present: (i) the LEP instrument in the solar wind (SW) mode, (ii) $T/N < 5$, where T and N are the proton temperature (keV) and density ($\rm cm^{-3}$), and (iii) high-speed plasma flows with $|V| > 500$ km/s. The criterion (ii) was demonstrated earlier [*Tsyganenko and Mukai*, 2003] to effectively discard remaining magnetosheath data records, undetected by the previous filtering based on a magnetopause model.

The final procedure was to convert the Geotail data into the GSW (Geocentric Solar Wind) coordinate system, taking into account the actual direction of the solar wind, observed at the time corresponding to a magnetospheric field measurement. The GSW coordinate system differs from the standard GSM only in that its X axis is directed anti-parallel to the observed solar wind flow, rather than to Sun's center, which more accurately

takes into account the variable aberration effect. To our knowledge, the GSW system was first introduced and described by *Hones et al.* [1986]. A detailed description of the coordinate transformation, converting vectors from GSM to GSW and back, was given by one of us earlier [*Tsyganenko et al.*, 1998] (being then unaware of Hones et al.'s work, we used there the notation GSMSW in place of GSW). Figure 2 shows the distribution of Geotail data used in this work, projected on the GSW equatorial and noon-midnight meridian planes. The total number of Geotail 5-min data records included in the final modeling set was 105,464.

2.2.2. Polar Data. Processing of the Polar MGF experiment data was in principle similar to that of Geotail, but because of the difference in the spatial coverage (much lower apogee) there was no need in the concurrent plasma data (which did not exist anyway). The purpose of including Polar observations was to properly sample the inner low-latitude magnetosphere; for that reason we selected from the outset only the data taken within a limited sector of solar-magnetic latitude between -30° and $+30^\circ$. We also did not include in the analysis the Polar data taken at $R < 3\,R_{\rm E}$, as irrelevant to the goal of this study. The data of Polar were also averaged over 5-min intervals; however, because it sampled much lower geocentric distances (where the main geomagnetic field and its gradient are much larger than at the Geotail location), the averaging was actually performed on the external part of the total field, after the internal (IGRF) field was subtracted from the total vector, and then the internal field corresponding to the center of the averaging interval was added back. Figure 3 illustrates the spatial distribution of the Polar data, included in the modeling dataset. Except for a different range of $\{X, Y, Z\}$ values, the plot is similar in its format to Figure 2, and the coordinate system used here is also the GSW. The total number of Polar 5-min average data records selected for the final dataset was 34,226.

3. Analytical Approximation for the Warped/Twisted Current Sheet

The shape of the current sheet was represented by the following equation, specifying the distance Z_N of the "neutral sheet" (a precise definition of the neutral sheet will be given below) from the GSW equatorial plane, as a function of X and Y (also in the GSW coordinates):

$$Z_N = -X\tan\Psi^* - G\sin\Psi\,F(Y, Y_1, \Delta Y) + S\left(\frac{-X}{10}\right)^T \frac{Y}{15}\frac{B_y}{5} \quad , \tag{1}$$

Three terms on the righthand side of (1) respectively represent (i) the solar-wind induced deflection of the neutral sheet from the tilted dipole equatorial plane, (ii) the tilt-related warping of the sheet in the Y-Z plane, and (iii) the twisting of the neutral sheet caused by the B_y component of the IMF.

The "effective" tilt angle Ψ^* in the first term is a function of the actual tilt angle Ψ and of the coordinate X (since our model is limited to the nightside, X is always negative):

$$\sin\Psi^* = \frac{\sin\Psi}{\left[1+\left(\frac{-X}{R_{\rm H}}\right)^{\alpha}\right]^{\frac{1}{\beta}}} \tag{2}$$

It also includes 3 parameters: the hinging distance $R_{\rm H}$, and the power indices α and $1/\beta$. The hinging distance defines the position of the bending on the neutral sheet surface, separating its near-Earth part (closely aligned with the dipole equatorial plane) from the more distant tailward region, where the neutral sheet gradually becomes parallel to the solar wind direction. The values of the parameters α and β define the sharpness of the transition region and the asymptotic position of the distant neutral sheet, as illustrated in Figure 4 (top). Larger values of both α and β provide a more abrupt bending of the sheet at the hinging location $X = -R_{\rm H}$, while smaller values yield a smoother transition. If $\alpha \leq \beta$, the neutral sheet monotonically departs from the GSW equatorial plane with growing tailward distance, but in the case $\alpha = \beta$ it asymptotically tends to become parallel to the Sun-Earth line. In the opposite case of $\alpha > \beta$, the distance between the neutral sheet and the equatorial plane is a non-monotonic function of X, so that at a sufficiently large $|X|$ the neutral sheet gradually returns back to the equatorial plane. The assumed form (2) of $\sin\Psi^*$ is a more flexible modification of a previously suggested approximation [*Tsyganenko*, 1998, Section 3, Eqs. (7)–(14); *Tsyganenko*, 2002a, Eqs. (7)–(12)].

The magnitude of the transverse warping as defined by the second term in (1) is controlled by the coefficient G, the sine of the dipole tilt angle Ψ, and the factor F, containing the dependence on the Y coordinate:

$$F = \tanh\frac{Y-Y_1}{\Delta Y} - \tanh\frac{Y+Y_1}{\Delta Y} + 2\,\tanh\frac{Y_1}{\Delta Y} \tag{3}$$

Approximation (3) includes two parameters, Y_1 and ΔY, whose meaning is illustrated in Figure 4 (bottom); the first one is the distance between the center of the transverse inflection of the neutral sheet and the midnight meridian plane, and the second one is a scale distance defining the relative steepness of the deformation. As was found earlier [*Tsyganenko et al.*, 1998], the transverse warping of the current sheet is the largest near Earth, but it

gradually decreases with growing distance. This effect can be easily taken into account by making the distance Y_1 in (3) linearly increase tailward as

$$Y_1 = Y_{10} + Y_{11}X \tag{4}$$

The third term in (1) describes the twisting of the neutral sheet due to the B_y component of the IMF. It linearly depends both on Y and IMF B_y and, since we expect the twisting angle to increase down the tail, it also includes a factor with a power dependence on the tailward distance. To keep the value of the model coefficient S on the order of unity, all three independent variables entering in the third term are divided by their characteristic scaling values (10, 15, and 5).

In comparison with previously used neutral sheet models, the adopted form (1)–(4) is more flexible. Combined with the dense data coverage of the modeling region, it has allowed us to accurately determine the shape of the tail current sheet, as detailed below.

4. Parameterization and Fitting to the Data

The approximation (1)–(4) for the global shape of the neutral sheet includes 9 parameters ($R_{\rm H}$, α, β, G, Y_{10}, Y_{11}, ΔY, S, and T), and uniquely defines Z_N as a function of X and Y, for any values of the dipole tilt Ψ and IMF B_y. In this study we aimed to derive not only an average tilt- and IMF B_y-dependent shape of the neutral sheet, but also its variation with the solar wind ram pressure $P_{\rm dyn}$ and IMF B_z component. A straightforward way for doing that is to represent the above 9 parameters as empirical functions of $P_{\rm dyn}$ and IMF B_z and then fit the model to the entire body of the data. However, as we did not have much apriori knowledge on the actual response of the model parameters to the solar wind and IMF state, our approach was twofold. First, a preliminary calculation was made of the model parameter dependence on the solar wind/IMF characteristics, by binning all the data into several intervals of $P_{\rm dyn}$ and IMF B_z and then fitting the 9 model parameters. The second step was to devise a "global" form of the model, containing suitable analytical approximations for those of the 9 parameters that showed an orderly bin-to-bin variation with either $P_{\rm dyn}$ or IMF B_z. The initial values of the model parameters were specified on the basis of the binning results, and a fitting procedure was then performed using the entire body of the data, as described below in more detail.

The fitting method was based on minimizing the number of mismatches between the observed orientation of the magnetic field and that predicted by the model. This approach was used in an early work by one of us [*Fairfield*, 1980], to derive the shape of the midtail neutral sheet at $X < -20\,R_{\rm E}$. In contrast to that effort, the present study addresses the global shape of the tail current sheet, including not only the middle tail with mostly sunward/antisunward **B** in the lobes, but also the near-Earth dawn and dusk sectors, where the magnetic field vector has a significant component in the Y-direction and the current sheet warps in two dimensions. Because of that, we need to accurately define the neutral sheet and choose a convenient criterion to determine the position of the spacecraft with respect to that sheet.

We define the neutral sheet as a warped surface, across which the tangential component of the **B** vector (calculated with respect to that surface) reverses its direction. Since the magnetotail current is flowing mostly in the azimuthal direction, the principal part of the **B** vector that reverses its orientation on crossing the sheet lies in the solar magnetic (SM) meridian plane. Based on that, we defined the neutral sheet as a surface at which

$$\mathbf{B} \cdot (\mathbf{n} \times \mathbf{e}_\phi) = 0 \quad , \tag{5}$$

where **n** is a unit normal vector to the surface and $\mathbf{e}_\phi$ is the unit vector in the direction of increasing SM longitude. The lefthand side of (5) approximately (to within a normalization factor on the order of unity) equals the magnitude of the field component lying in the plane of the SM meridian and tangential to the neutral sheet. It can be calculated from the observed field vector and the neutral sheet model (1)–(4), and we use its sign as an indicator of the spacecraft position with respect to the warped neutral sheet. Even though we do not know the distance of the observation point from the neutral sheet, we still can project it on the sheet along the Z axis and calculate there the direction of the normal vector **n** (since it does not depend on Z) as

$$\mathbf{n} = \frac{\nabla \Phi}{|\nabla \Phi|} \quad , \tag{6}$$

where the scalar function $\Phi = Z - Z_N$ is defined by the neutral sheet model (1)–(4), and then determine the sign of the lefthand side of (5). Positive (negative) values of $\mathbf{B} \cdot (\mathbf{n} \times \mathbf{e}_\phi)$ indicate that the observation point is located northward (southward) from the model neutral sheet. If the sign of $\mathbf{B} \cdot (\mathbf{n} \times \mathbf{e}_\phi)$ is the same as of $\Phi = Z - Z_N$, then the model prediction matches the observation, otherwise we have a mismatch. The total percentage Q of

mismatches over the entire dataset was used as a target function of the neutral sheet model. By making a search in the model parameter space, we minimized Q and obtained a best-fit representation of the neutral sheet. Note that the method does not use least squares and, hence, neither there was a straightforward way to linearize the problem nor any straightforward method to estimate the uncertainties of the best-fit parameter values. For that reason, instead of applying a standard inversion technique, we derived the model parameters by using a version of the simplex algorithm, and estimated the uncertainties using a bootstrap method [*Press et al.*, 1992, Ch. 10.4, 15.6; *Efron and Tibshirani*, 1993, Ch.6].

5. Results

Tables 1 and 2 present the results of the preliminary study where the 9 model parameters were calculated for 5 bins of the solar wind ram pressure P and for 8 bins of the IMF B_z (GSM) component. The following trends become apparent from inspecting the parameter values. (1) The hinging distance $R_{\rm H}$ steadily decreases with growing P, while the transverse warping amplitude G increases. (2) Whereas β is slightly smaller for positive IMF B_z, the parameter α gets larger, so that their difference $\alpha - \beta$ varies from -0.4 for IMF $B_z < -6$ nT, to $+0.7$ for IMF $B_z > +6$ nT. (3) Both twisting parameters, S and T, clearly increase with growing positive IMF B_z. Based on these facts, we adopted the following approximations for the parameters $R_{\rm H}$, G, β, S, and T:

$$R_{\rm H} = R_{H0}\left(\frac{P}{\langle P\rangle}\right)^{\chi_{R_{\rm H}}} \qquad G = G_0\left(\frac{P}{\langle P\rangle}\right)^{\chi_G} \qquad \beta = \beta_0 + \beta_1\ \tanh\left(\frac{B_z - B_{z\beta}}{\Delta B_{z\beta}}\right)$$
$$S = S_0 + S_1\ \tanh\left(\frac{B_z}{\Delta B_{z_{ST}}}\right) \qquad T = T_0 + T_1\ \tanh\left(\frac{B_z}{\Delta B_{z_{ST}}}\right) \tag{7}$$

All other parameters entering in (1)–(4) exhibited less orderly dependence on P and B_z, and hence were treated just as unknown constants, whose best-fit values were also found from the data. Equations (1)–(4) and (7) provide an exhaustive formulation of the neutral sheet model, and Table 3 summarizes the results of its fitting to the entire set of Geotail and Polar data, along with the values of uncertainties. The uncertainties were estimated using the bootstrap method, based on a number of resampled subsets with the same number of data records as in the original dataset, but with a fraction of the data being randomly replaced by duplicated original records. In this

particular realization of the bootstrap approach, we created 25 random subsets and calculated the uncertainties of individual parameters from the range of the dispersion of their 25 best-fit values.

The average shape of the neutral sheet and its dependence on the solar wind and IMF, as derived from the model, is illustrated in Figures 5–7, each showing a family of cross-sections of the sheet by equidistant planes $X = -5, -10, -15, ..., -50\, R_{\rm E}$. The effect of the solar wind pressure P on the tilt-related warping of the neutral sheet can be clearly seen in Figure 5, comparing the shapes for an average $P = 2$ nPa (top) and relatively large $P = 6$ nPa (bottom) value of the pressure. Both panels correspond to the maximal positive value of the tilt angle $\Psi = 35^\circ$ and IMF $B_y = 0$. As can be seen from the plots, the decrease of the hinging distance with growing solar wind pressure results in a lesser amplitude of the north-south motion of the neutral sheet near the midnight meridian for $P = 6$ nPa. At the same time, the increase of the warping amplitude G with growing P results in a larger amplitude of the oppositely directed shift of the neutral sheet at the flanks of the near-Earth tail. At larger tailward distances, owing to the linear increase of Y_1 in (3)–(4), the neutral sheet gradually flattens, so that in the midtail ($X \sim -50\, R_{\rm E}$) the reversal from northward to southward motion occurs at a much larger distance from the midnight meridian than in the near tail.

Figure 6, similar in format to Fig. 5, demonstrates the effect of the IMF B_z by comparing the shapes of the warped model neutral sheet for the same values of $\Psi = 35^\circ$, $P = 2$ nPa, and IMF B_y, but for two opposite polarities of IMF B_z, equal to -10 nT (top) and $+10$ nT (bottom). As clearly seen, negative IMF B_z results in a more gradual bending of the neutral sheet in the near tail, and, hence, significantly larger amplitude of the north-south motion of the sheet in the midtail. This can be viewed as a consequence of a larger magnetic flux in the tail lobes during periods of southward IMF, and hence a less flexible tail, more rigidly tied to the tilted dipole. As demonstrated below, this interpretation is consistent with a similar effect of the IMF B_z on the IMF B_y-related twisting.

Figure 7 displays a family of neutral sheet cross-sections for untilted dipole, average $P = 2$ nPa, but non-zero IMF $B_y = 10$ nT, illustrating the counter-clockwise twisting of the sheet around the GSW X-axis. As in the previous figure, top and bottom panels corresponds to IMF $B_z = -10$ nT and $+10$ nT, respectively. A dramatically larger degree of the twisting in the latter case fully agrees with earlier findings [*Owen,* 1995;

Maezawa et al., 1997], and confirms much larger susceptibility of the tail to external stresses induced by the IMF during periods with northward polarity.

6. Discussion and Conclusions

It is interesting to compare the results of this study with our earlier empirical model [*Tsyganenko et al.*, 1998]. That model was based on a smaller set of Geotail data, binned into 7 intervals of X, and used a completely different fitting method. Figure 8 compares the shape of the warped neutral sheet cross sections for $\Psi = 35^\circ$ at 6 different tailward distances, corresponding to the centers of 6 first bins of the $X_{\rm GSW}$ coordinate. Solid and dotted lines correspond, respectively, to the present (Eqs. (1)–(4)) and the old model. The values of the solar wind parameters in the new model were assumed equal to their average values: $P = 2$ nPa, and IMF $B_y = B_z = 0$. The agreement between the two approximations is fairly good in the near and middle tail ($X_{\rm GSW} \geq -35\, R_{\rm E}$), where the deviation between model surfaces is typically within $1.0 - 1.5\, R_{\rm E}$. At larger tailward distances the new model predicts systematically larger deflection of the neutral sheet from the GSW equatorial plane, than according to the old model, especially near the dawn and dusk sides of the tail, where the discrepanies rise to $\sim 3\, R_{\rm E}$.

Figure 9, similar in its format to Figure 8, compares the twisting effect of the IMF B_y, as reproduced by the new and old approximations. Here the dipole tilt angle was assumed zero, $P = 2$ nPa, IMF $B_y = 10$ nT, and $B_z = 0$. In general, the new model predicts larger twisting angles at all distances. Note that the old approximation for Z_N included a quadratic term with respect to Y, introduced in order to take into account a possible S-shaped deformation of the current sheet. As can be seen from the plot, such a nonlinear distortion was found to be significant only in the nearest bin of X, but it remained unclear if that was a real effect or just a modeling artifact. In this work, we restricted the model to only a linear dependence of Z_N on Y, which ignored the possibility of the S-shaped twisting of the neutral sheet by retaining only the principal linear term. The closest agreement between the models was found for $X = -22.5\, R_{\rm E}$ (3rd panel from bottom of the plot), where the solid and dotted lines almost coincide. At larger tailward distances the discrepancy steadily increases and becomes quite significant at $X = -50\, R_{\rm E}$, where the new model predicts the rotation almost twice as large as in

the old one.

To give readers a clearer sense of the general range of the neutral sheet deformation, we reproduce in Figure 10 a 3D view of the model surface, calculated from (1)–(4) and (7) for $\Psi = 35\,^{\circ}$ and IMF $B_y = -10$ nT. The solar wind pressure and IMF B_z were assumed equal to their average values $P = 2$ nPa and $B_z = 0$.

In summary, we developed a new analytical approximation for the global shape of the tail neutral sheet, parameterized by the tilt of the Earth's dipole, solar wind pressure, and the transverse components of the IMF, B_y and B_z. Numerical values of the model parameters were found by minimizing the total number of mismatches between the predicted and observed orientation of the magnetic field, based on 9 years of Geotail and 3 years of Polar data, taken in the proximity of the tail's plasma sheet.

The model is valid within the nightside magnetosphere in the range of tailward distances $-50\,R_{\rm E} \leq X_{\rm GSM} \leq 0$. Variations of the solar wind pressure P change the shape of the deformed current sheet in such a way that an increase of P results in a decrease of the magnetotail "hinging distance" $R_{\rm H}$, but increases the magnitude of its transverse warping. The IMF B_z component affects the magnitude of the seasonal/diurnal motion of the current sheet in the north-south direction, and it also controls the degree of the IMF B_y-related twisting, which becomes much larger during the periods with northward IMF B_z, in agreement with earlier published studies.

Acknowledgments. It is a pleasure to acknowledge the teams and PIs of all experiments, whose data were used in this study. Geotail MGF data were provided by the PIs, S. Kokubun (STEL) and T. Nagai (Tokyo Institute of Technology, Japan). The data of Polar MGF experiment were made available by the UCLA team led by the PI C. T. Russell. Interplanetary medium data of Wind (K. Ogilvie and R. Lepping, NASA GSFC), IMP 8 (A. Lazarus, MIT, and R. Lepping, NASA GSFC), and ACE (D. McComas, LANL, and N. Ness, Bartol Research Institute) were obtained from NSSDC via CDAWEB online facility. This work was supported by NSF grants ATM-0296212 and by NASA's LWS grant NAG5-12185.

References

Dandouras, J., On the average shape and position of the geomagnetic neutral sheet and its influence on plasma sheet ststistical studies, *J. Geophys. Res., 93,* 7345, 1988.

Efron, B., and R. Tibshirani, *An introduction to the bootstrap*, Chapman and Hall, New York, 1993.

Fairfield, D. H., A statistical determination of the shape and position of the geomagnetic neutral sheet, *J. Geophys. Res., 85,* 775–780, 1980.

Gosling, J. T., D. J. McComas, M. F. Thomsen, S. J. Bame, and C. T. Russell, The warped neutral sheet and plasma sheet in the near-Earth geomagnetic tail, *J. Geophys. Res., 91,* 7093, 1986.

Hones, E. W., R. D. Zwickl, T. A. Fritz, and S. J. Bame, Structural and dynamical aspects of the distant magnetotail determined from ISEE-3 plasma measurements, *Planet. Space Sci., 34,* 889, 1986.

Lopez, R.E., The position of the magnetotail neutral sheet in the near-Earth region, *Geophys. Res. Lett., 17,* 1617, 1990.

Maezawa, K., T. Hori, T. Mukai, Y. Saito, T. Yamamoto, S. Kokubun, and A. Nishida, Structure of the distant magnetotail and its dependence on the IMF B_y component: Geotail observations, *Adv. Space Res., 20,* 949, 1997.

Owen, C. J., J. A. Slavin, I. G. Richardson, N. Murphy, and R. J. Hynds, Average motion, structure and orientation of the distant magnetotail determined from remote sensing of the edge of the plasma sheet boundary layer with $E > 35$ keV ions, *J. Geophys. Res., 100,* 185–204, 1995.

Press, W. H., S. A. Teukolsky, W. T. Vetterling, and B. P. Flannery, *Numerical Recipes,* 2nd ed., Cambridge Univ. Press, New-York, 1992.

Richardson, J. D., and K. I. Paularena, Plasma and magnetic field correlations in the solar wind, *J. Geophys. Res., 106,* 239, 2001.

Russell, C. T., The configuration of the magnetosphere, in *Critical Problems of Magnetospheric Physics,* edited by E. R. Dyer, pp.1–16, IUCSTP Sec., Nat. Acad. of Sci., Washington, D. C., 1972.

Russell, C. T., and K. I. Brody, Some remarks on the position and shape of the neutral sheet, *J. Geophys. Res., 72,* 6104–6106, 1967.

Shue, J.-H., et al., Magnetopause location under extreme solar wind conditions, *J. Geophys. Res., 103,* 17,691, 1998.

Sibeck, D. G., G. L. Siscoe, J. A. Slavin, E. J. Smith, B. T. Tsurutani, and R. P. Lepping, The distant magnetotatil's response to a strong interplanetary magnetic field B_y: Twisting, flattening, and field line bending, *J. Geophys. Res., 90,* 4011–4019, 1985.

Tsyganenko, N. A., Modeling of twisted/warped magnetospheric configurations using the general deformation method, *J. Geophys. Res.*, *103*, 23,551, 1998.

Tsyganenko, N. A., A model of the near magnetosphere with a dawn-dusk asymmetry 1. Mathematical structure, J. Geophys. Res., v.107 (A8), doi: 10.1029/2001JA000219, 2002a.

Tsyganenko, N. A., A model of the near magnetosphere with a dawn-dusk asymmetry 2. Parameterization and fitting to observations, J. Geophys. Res., v.107 (A8), doi: 10.1029/2001JA000220, 2002b.

Tsyganenko, N. A., S. B. P. Karlsson, S. Kokubun, T. Yamamoto, A. J. Lazarus, K. W. Ogilvie, and C. T. Russell, Global configuration of the magnetotail current sheet as derived from Geotail, Wind, IMP 8, and ISEE 1/2 data, *J. Geophys. Res.*, *103*, 6827–6842, 1998.

Tsyganenko, N. A., G. Le, C. T. Russell, and T. Iyemori, A study of the inner magnetosphere based on data of Polar, *J. Geophys. Res.*, *104*, 10,275, 1999.

Tsyganenko, N. A., and T. Mukai, Tail plasma sheet models derived from Geotail particle data, *J. Geophys. Res.*, *108*, 1136, doi:10.1029/2002JA009707, 2003.

N. A. Tsyganenko, Universities Space Research Association, Code 695, Laboratory for Extraterrestrial Physics, NASA Goddard Space Flight Center, Greenbelt, MD 20771. (Nikolai.Tsyganenko@gsfc.nasa.gov)

D. H. Fairfield, Laboratory for Extraterrestrial Physics, NASA Goddard Space Flight Center, Greenbelt, MD 20771. (Donald.H.Fairfield@nasa.gov)

Received ... , 2001; revised ...., 2003; accepted ....., 2003.

Submitted to the *Journal of Geophysical Research*, 2003.

Figure 1. Distribution of the deviation Θ of the observed solar wind flow from its average direction, calculated using 5-min averages of IMP 8, Wind, and ACE data taken between 1994 and 2002. The total number of data records used for plotting this histogram is 643,568. Vertical dashed lines show the 5% (left), median (center), and 95% (right) values of Θ.

Figure 2. Spatial coverage of the low-latitude magnetosphere by Geotail data used in this study, shown in the GSW equatorial (top) and noon-midnight meridional (bottom) projections. Each dot corresponds to a 5-min average data record, whose total number equals 105,464.

Figure 3. Spatial coverage of the low-latitude inner magnetosphere by Polar data used in this study, shown in the GSW equatorial (top) and noon-midnight meridional (bottom) projections. Each dot corresponds to a 5-min average data record, and their total number equals 34,226.

Figure 4. Illustrating the model approximation (1)–(4) for the global shape of the neutral sheet: (top) midnight meridian sections of the deformed neutral sheet for different values of the parameters α and β; (bottom) the shape of the warped neutral sheet in the tail cross section ($X = -15\,R_{\rm E}$), and an illustration of the model parameters Y and ΔY. The plots correspond to the maximal value of the dipole tilt angle $\Psi = 35\,^\circ$. Outer part of the model surface lying outside the magnetopause is shown in the bottom panel by dashed line.

Figure 5. Comparing the shapes of the warped neutral sheet for average (top) and large (bottom) values of the dynamic pressure of the solar wind. Families of cross sections in each panel correspond to equidistant planes, crossing the Sun-Earth line at $X = -5, -10, -15, ..., -50\,R_{\rm E}$. The endpoints of the near-tail contours that do not reach the plot frames correspond to the position of the model magnetopause of *Shue et al.* [1998].

Figure 6. Same as in Figure 5, but for two opposite polarities of the IMF B_z: (top) $B_z = -10$ nT and (bottom) $B_z = +10$ nT.

Figure 7. Illustrating the effect of the IMF B_y-related twisting of the neutral sheet and its dependence on the IMF B_z, using the same format as in Figures 5 and 6. In this example IMF $B_y = 10$ nT. Note a strikingly larger twisting in the case of northward IMF B_z.

Figure 8. Illustrating the 3D shape of the model warped neutral sheet for $\Psi = 35\,^\circ$ (solid contours) in comparison with our earlier result (dotted lines).

Figure 9. Same as in Figure 8, but for the twisting effect by the IMF $B_y = 10$ nT, with zero geodipole tilt.

Figure 10. A three-dimensional view of the warped and twisted tail neutral sheet, obtained for $\Psi = 35\,^{\circ}$, IMF $B_y = -10\,$nT, $P = 2\,$nPa, and IMF $B_z = 0$.

Table 1. Parameters of the Model Neutral Sheet From Subsets of Data for 5 Bins of the Solar Wind Pressure.

P (nPa)	$[0,1]$	$[1,2]$	$[2,3]$	$[3,4]$	>4
$R_{\rm H}$	12.6	11.6	10.5	9.5	9.1
α	2.20	2.25	2.19	2.17	2.13
β	1.94	1.96	1.90	1.90	1.97
G	24.0	26.4	26.7	29.5	29.5
Y_{10}	16.5	17.1	16.5	16.4	16.7
Y_{11}	-.244	-.239	-.236	-.193	-.280
ΔY	6.85	6.76	6.73	6.34	7.18
S	0.78	0.85	0.75	0.75	0.46
T	0.73	0.82	0.81	0.78	0.82

Table 2. Parameters of the Model Neutral Sheet From Subsets of Data for 8 Bins of the IMF B_z.

B_z (nT)	< -6	$[-6, -4]$	$[-4, -2]$	$[-2, 0]$	$[0, 2]$	$[2, 4]$	$[4, 6]$	> 6
$R_{\rm H}$	9.85	11.2	10.9	10.3	10.2	10.3	10.0	10.2
α	1.84	2.43	2.35	2.24	2.15	2.32	2.89	2.75
β	2.22	2.33	2.13	1.97	1.94	2.00	2.04	2.04
G	21.4	27.8	28.2	25.1	27.0	28.7	29.5	27.9
Y_{10}	18.7	17.7	17.5	16.7	16.6	17.1	17.2	17.0
Y_{11}	-.123	-.242	-.264	-.265	-.244	-.215	-.206	-.165
ΔY	9.77	7.52	7.46	7.06	6.56	6.56	6.70	6.60
S	0.58	0.60	0.58	0.73	0.76	0.84	0.86	1.28
T	0.80	0.70	0.63	0.72	0.76	0.93	0.94	1.18

Table 3. Global Parameters of the Model Neutral Sheet, Entering in (1)–(4), and (7)

Parameter	Value	Uncertainty
R_{H0}	9.956	±0.095
$\chi_{R_{\rm H}}$	-0.209	±0.086
α	2.113	±0.029
β_0	1.986	±0.025
β_1	-0.198	±0.025
$B_{z\beta}$	2.122	±0.61
$\Delta B_{z\beta}$	3.233	±0.86
G_0	26.90	±0.45
χ_G	0.227	±0.064
Y_{10}	17.21	±0.082
Y_{11}	-0.215	±0.005
ΔY	6.916	±0.074
S_0	0.745	±0.025
S_1	0.297	±0.056
$\Delta B_{z_{ST}}$	4.08	±0.85
T_0	0.840	±0.041
T_1	0.222	±0.046

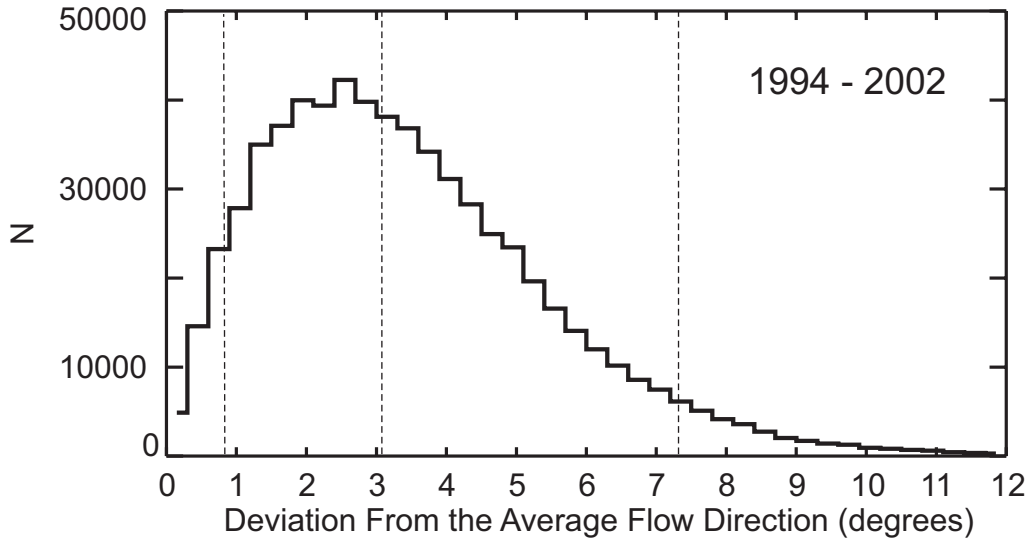
50000
30000
10000
0
N
1994 - 2002
0
1
2
3
4
5
6
7
8
9
10
11
12
Deviation From the Average Flow Direction (degrees)

Figure 1

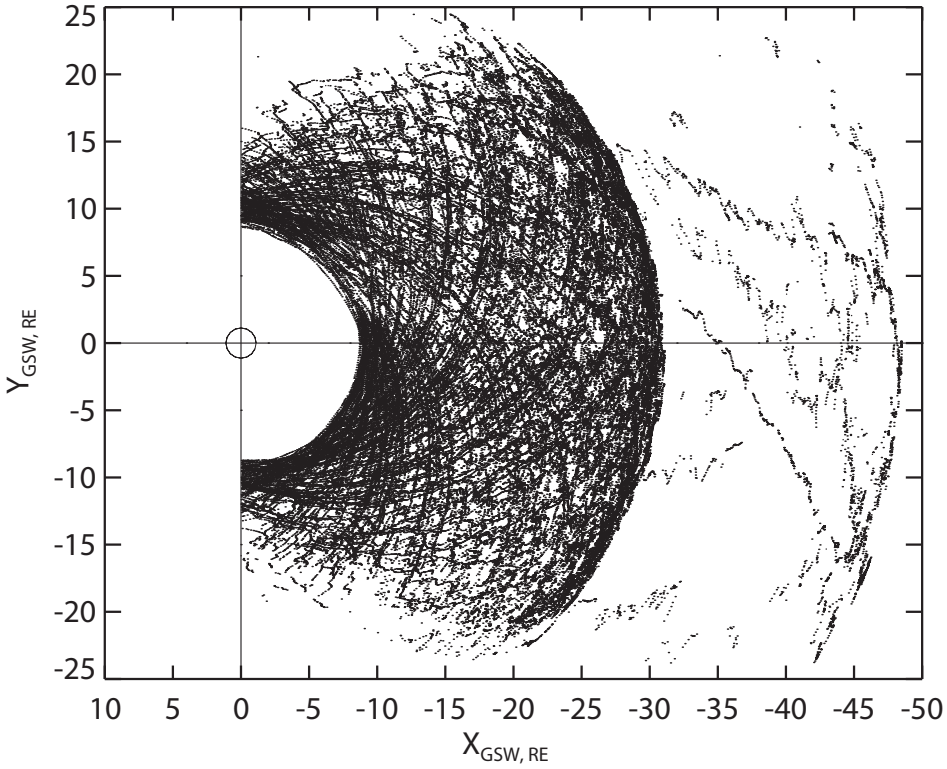
25
20
15
10
5
0
-5
-10
-15
-20
-25
$Y_{GSW, RE}$
10
5
0
-5
-10
-15
-20
-25
-30
-35
-40
-45
-50
$X_{GSW, RE}$

Figure 2a

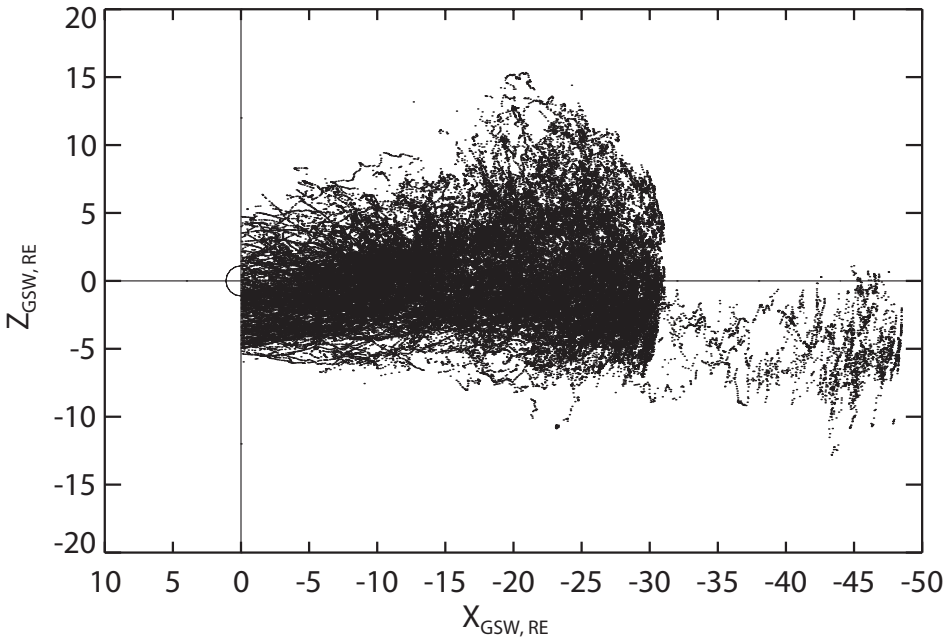
20
15
10
5
0
-5
-10
-15
-20
$Z_{GSW, RE}$
10
5
0
-5
-10
-15
-20
-25
-30
-35
-40
-45
-50
$X_{GSW, RE}$

Figure 2b

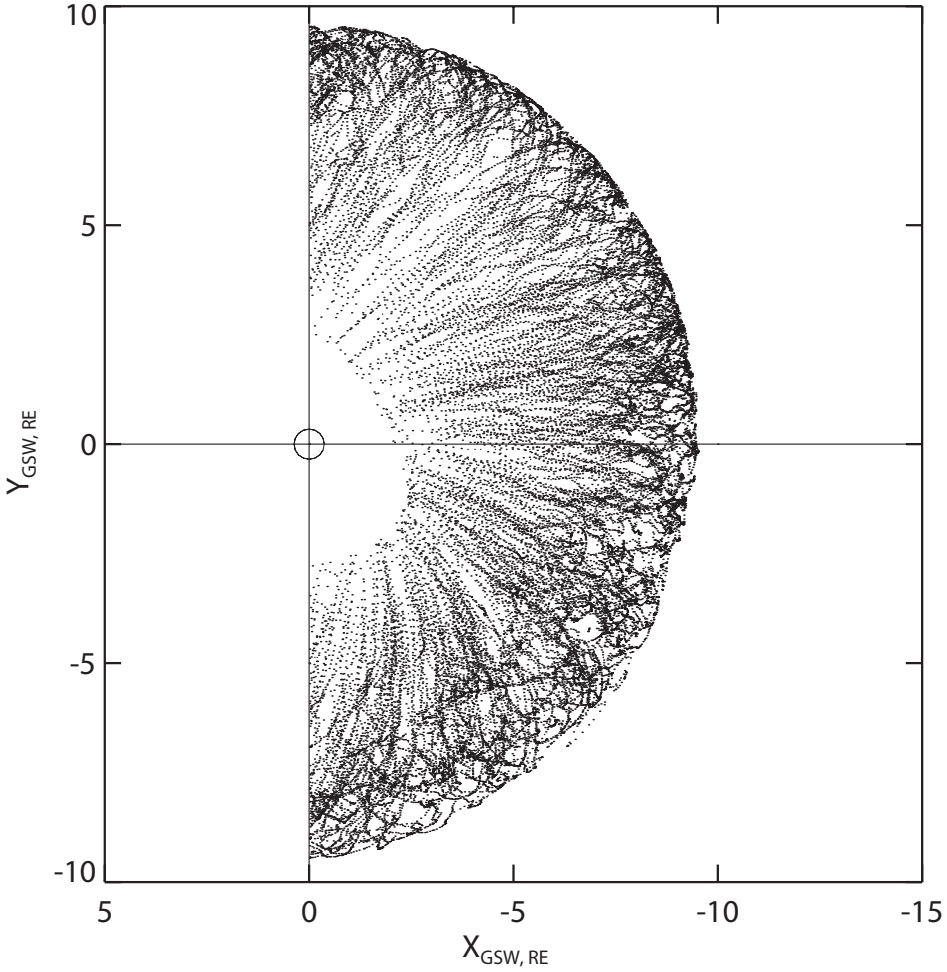

Figure 3a

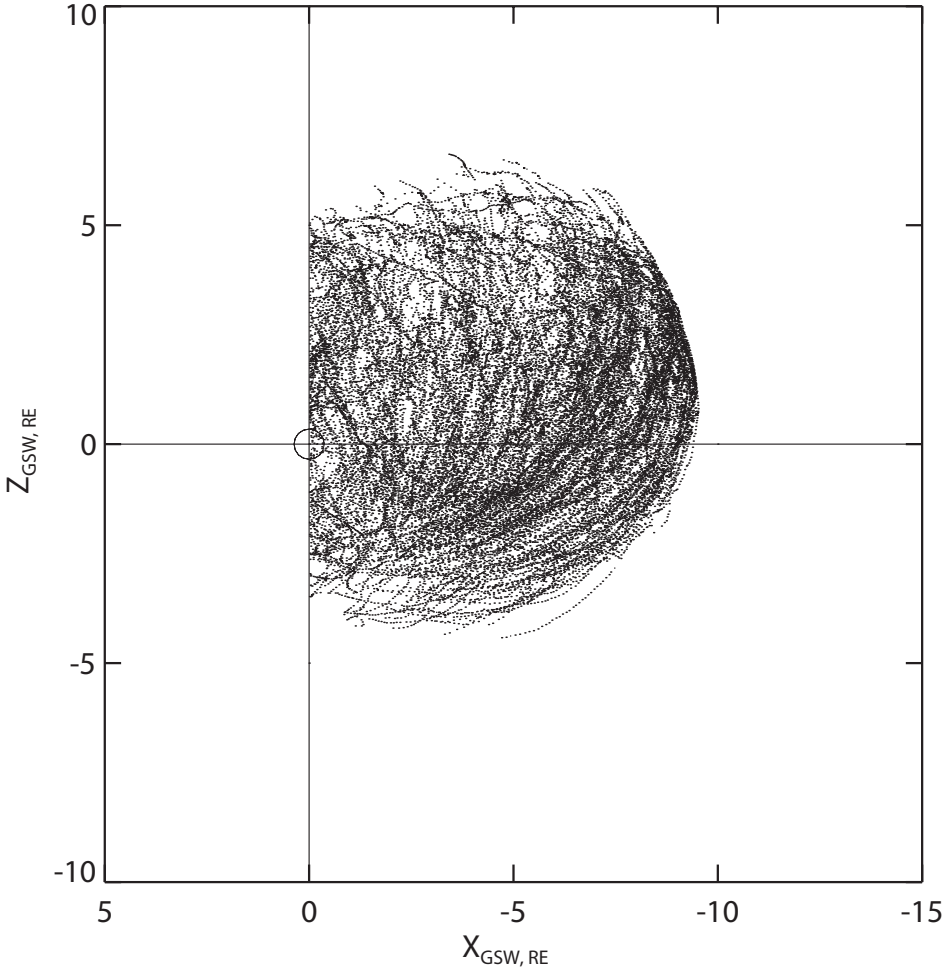

Figure 3b

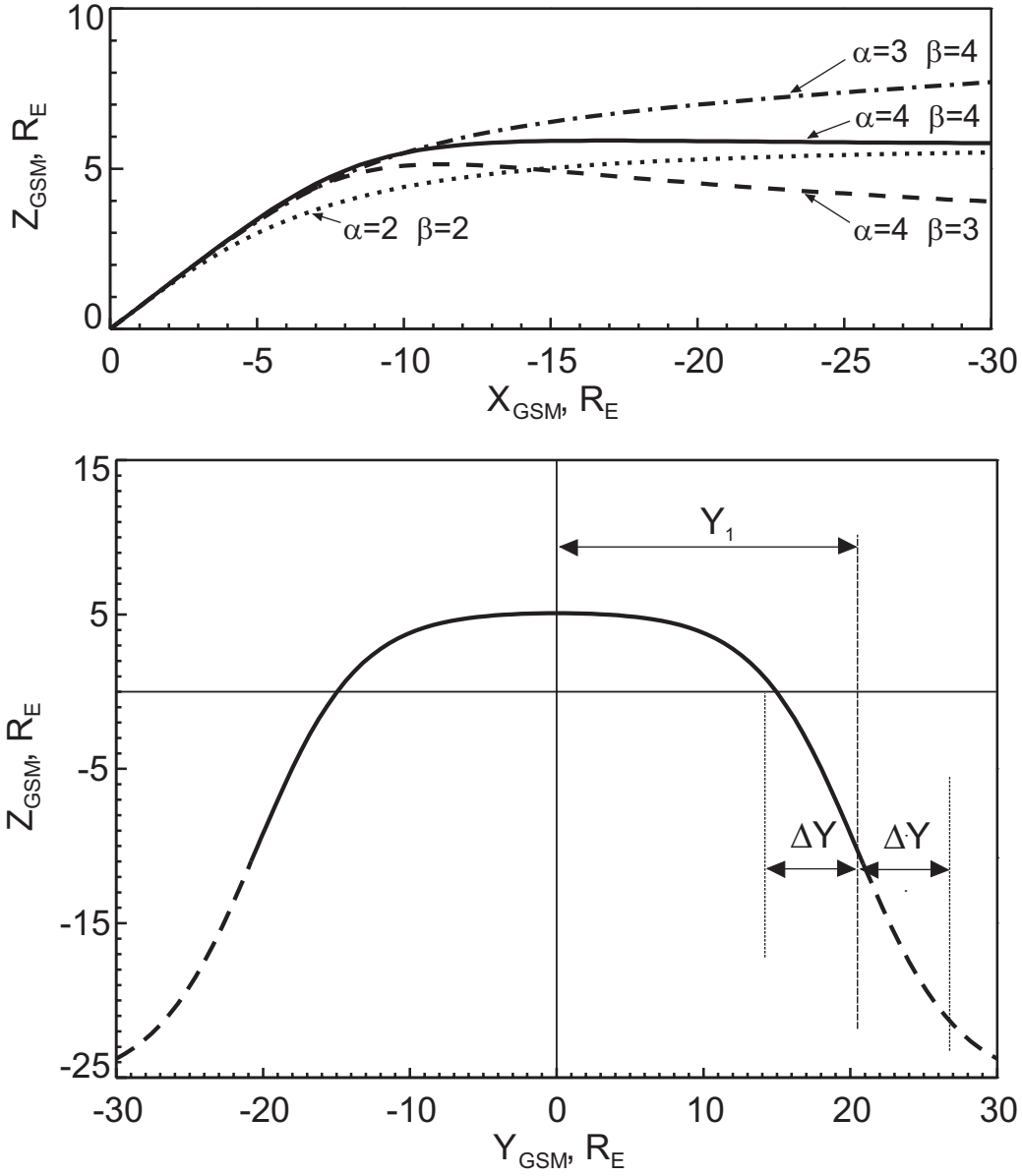
10
5
0
Z_{GSM}, R_E
α=3 β=4
α=4 β=4
α=2 β=2
α=4 β=3
0
-5
-10
-15
-20
-25
-30
X_{GSM}, R_E
15
5
-5
-15
-25
Z_{GSM}, R_E
Y_1
ΔY
ΔY
-30
-20
-10
0
10
20
30
Y_{GSM}, R_E

Figure 4

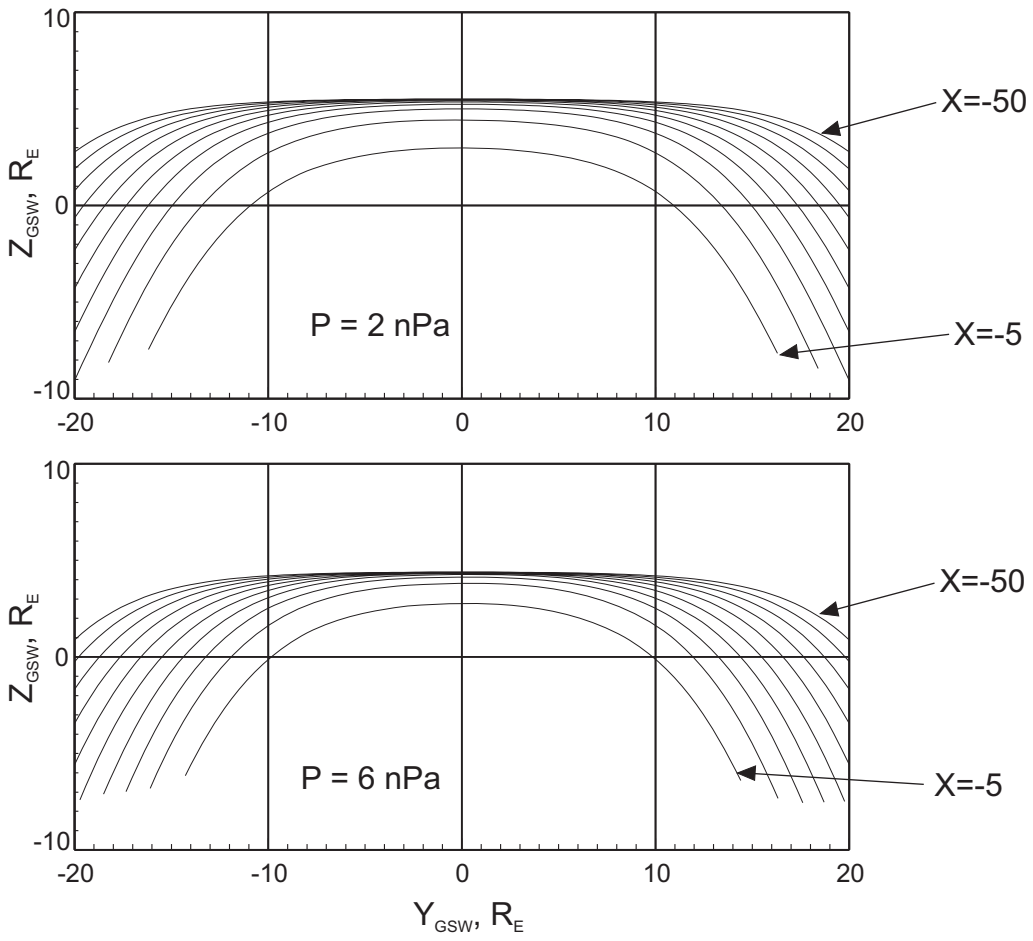
10
0
-10
-20
-10
0
10
20
Z_{GSW}, R_E
P = 2 nPa
X=-50
X=-5
10
0
-10
-20
-10
0
10
20
Z_{GSW}, R_E
P = 6 nPa
X=-50
X=-5
Y_{GSW}, R_E

Figure 5

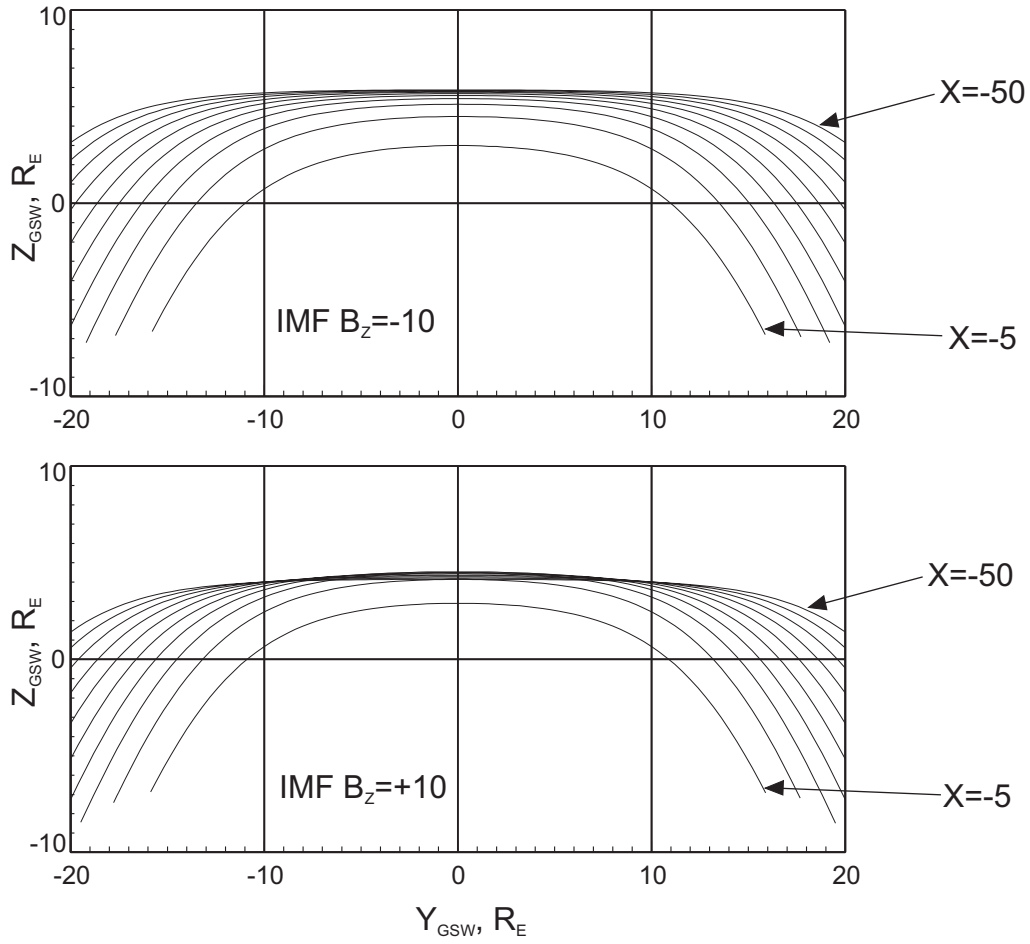

Figure 6

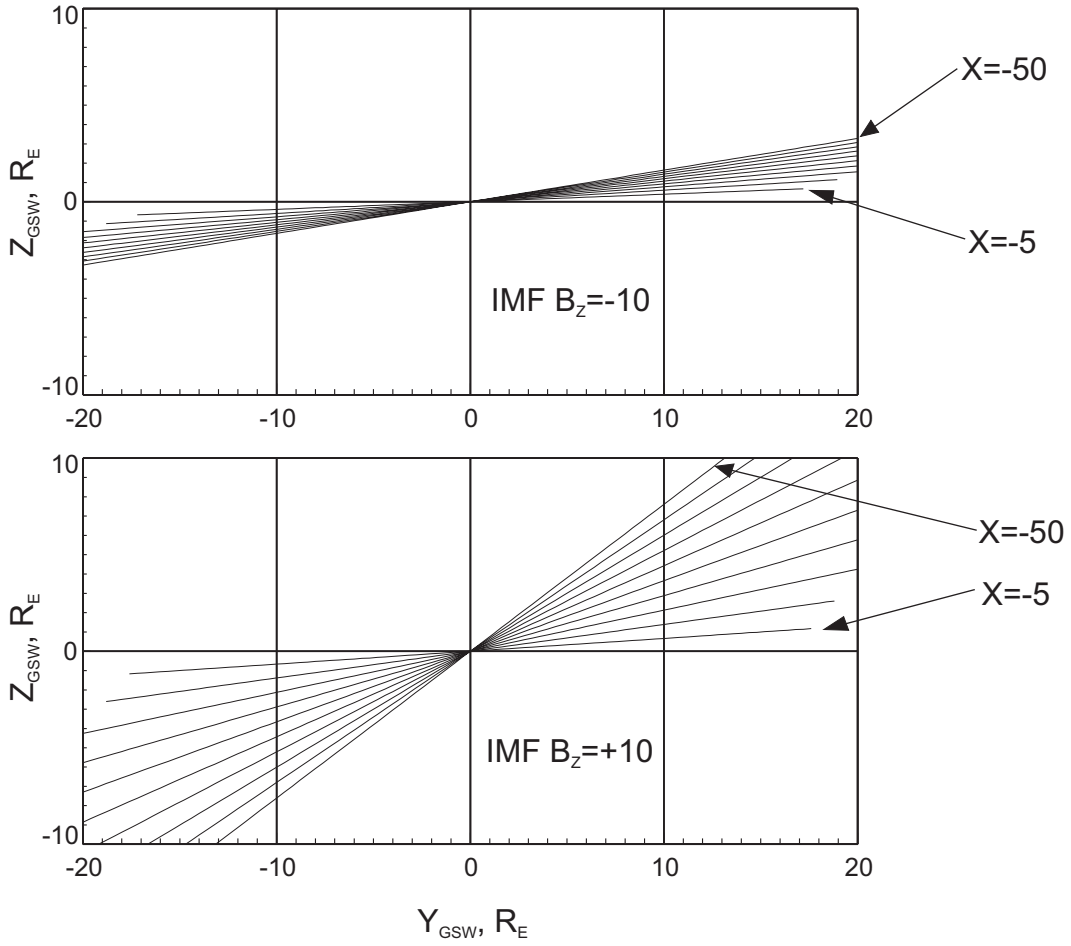

Figure 7

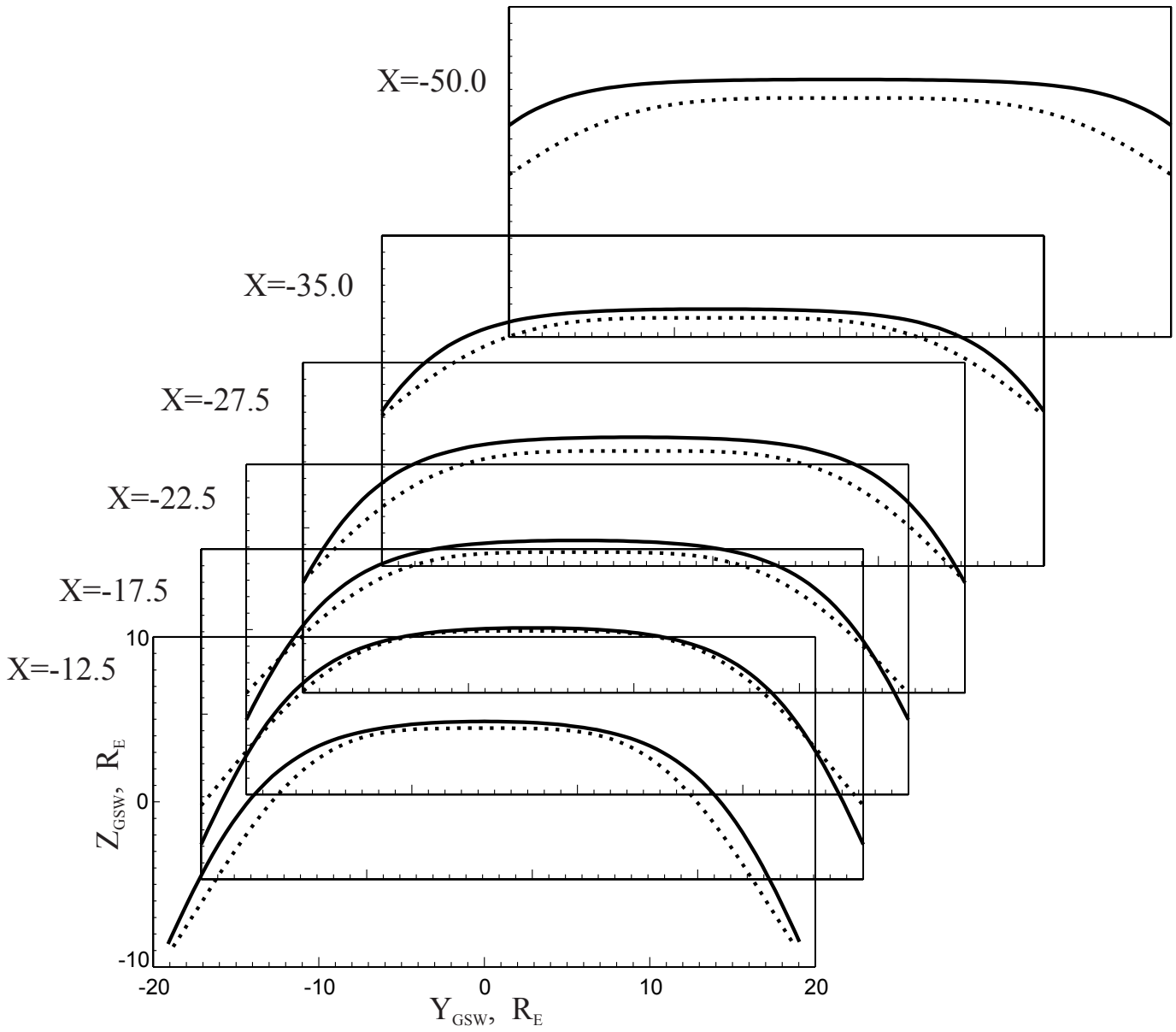
X=-50.0
X=-35.0
X=-27.5
X=-22.5
X=-17.5
X=-12.5
10
0
-10
-20
-10
0
10
20
Z_{GSW}, R_E
Y_{GSW}, R_E

Figure 8

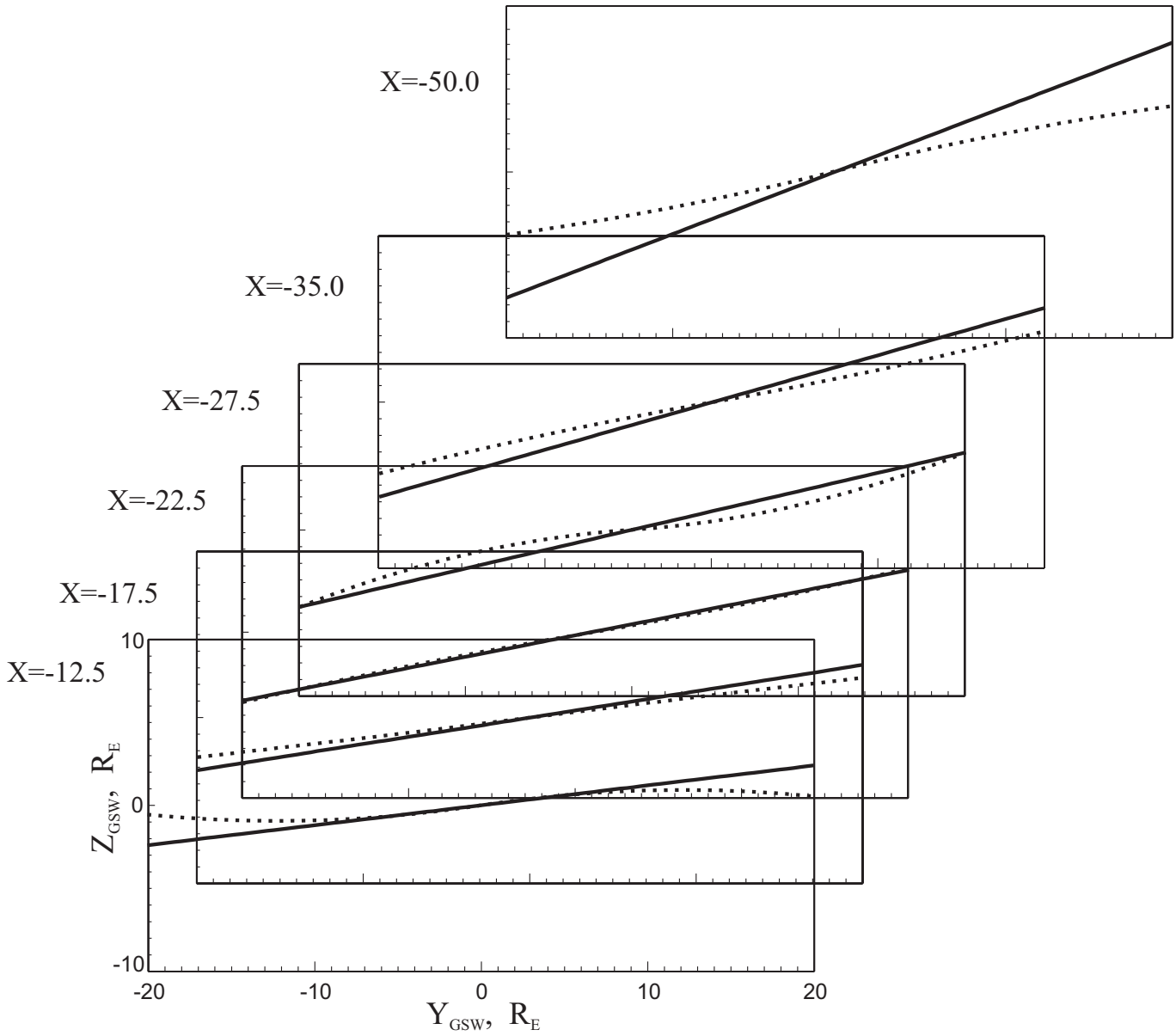
X=-50.0
X=-35.0
X=-27.5
X=-22.5
X=-17.5
X=-12.5
10
0
-10
Z_{GSW}, R_E
-20
-10
0
10
20
Y_{GSW}, R_E

Figure 9

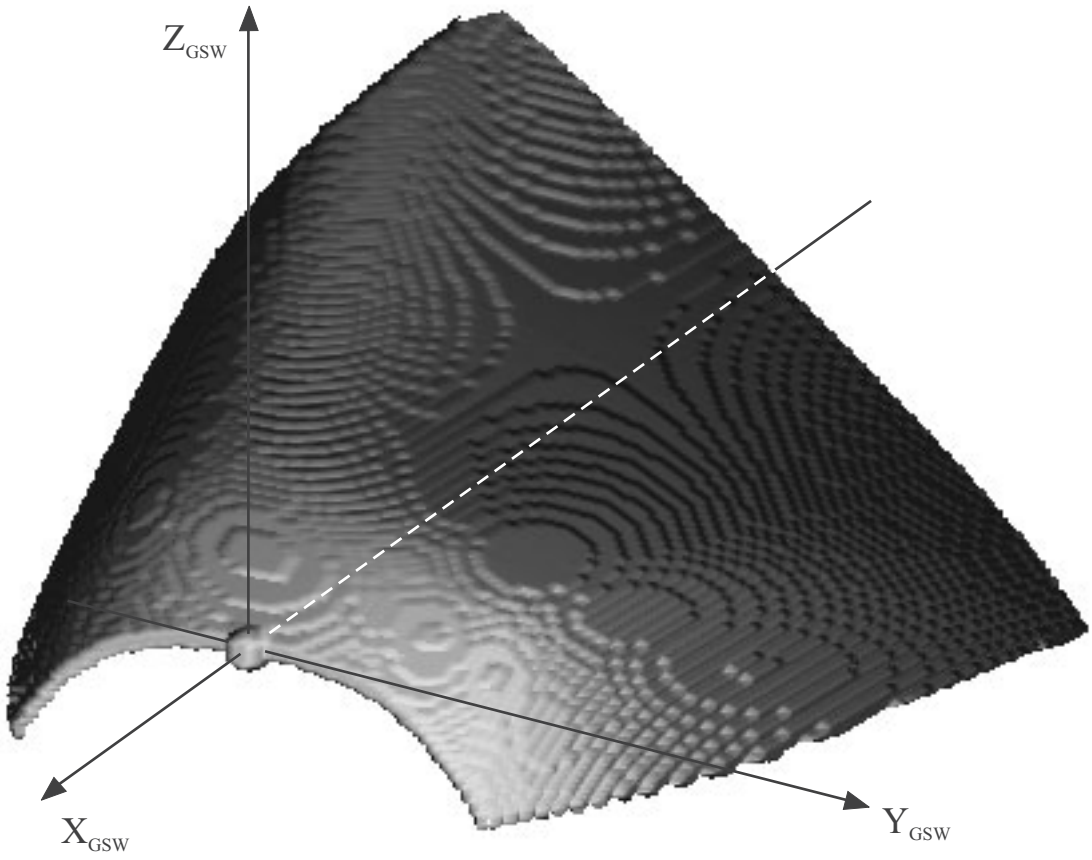

Figure 10